Field Characterization of Location-specific Dynamic Amplification Factors towards Fatigue Calculations in Ship Unloaders

G. Milana
Lloyd's Register Global Technology Centre, Southampton, UK and UCD, Belfield, Dublin 4, Ireland

K. Banisoleiman
Lloyd's Register Global Technology Centre, Southampton, UK

A. González
University College Dublin (UCD), Belfield, Dublin 4, Ireland

ABSTRACT: This paper highlights the impact of dynamic amplification factors in remaining fatigue life assessment of ship unloaders. In practice, the widely accepted procedure for these structures is to carry out a fatigue life assessment envisages: (1) carrying out static analysis, (2) taking into account dynamics via the application of dynamic amplification factors, and (3) applying Miner's rule. This factor, provided by the standard, is applied to the structure as a whole without considering the vibration of each structural member individually. This paper characterizes the dynamic behavior of each element using location-based dynamic amplification factors estimated from measurements. This caters for a more accurate assessment of the structure, whilst maintaining the simplicity of the standard procedure.

1 INTRODUCTION

Given the key role of ship unloaders in the marine cargo transport system and their arduous working environment, it is crucial to accurately assess their residual life to ensure safe and un-interrupted operation. Even though these structures are subject to continuous hoisting cycles, which induce alternating stresses in the structural members, surprisingly only static analyses are carried out as the basis when assessing their fatigue life (Milana 2016a, 2016b). In fact, the basic conventional procedure consists of the following three steps:
(1) carry out a static analysis for different load cases, corresponding to different position of the loaded grab and shuttle trolley, based on a Finite Element (FE) model of the structure calibrated with field measurements,
(2) take dynamic effects into account by applying a Dynamic Amplification Factor (DAF) to the static stresses in (1). DAF is defined here as the ratio of the maximum total response (i.e., 'static' + 'dynamic') to the maximum static response, and
(3) estimate fatigue life using Miner's rule based on the stress ranges obtained in (2).

The value of DAF in step (2) is typically adopted from the Federation Europeenne de la Manutention (FEM 1.001), which establishes that DAF depends on the type of crane and on the hoisting speed. The chart in Figure 1 plots the value of DAF (i.e., Ψ in the vertical axis) versus the hoisting speed (i.e., $\mathbf{V_L}$ in the horizontal axis, expressed in m/s). The line 'A' refers to overhead travelling cranes and bridge cranes, while 'B' to jib cranes. Ψ is a global DAF that makes no distinction between different crane sections or stress ranges. Although such an approach may be conservative, it is not realistic, since some sections or stress ranges can be more prone to dynamic amplification than others. For example, the waterside ties in ship unloaders, show a highly dynamic behavior that cannot usually be represented through static analysis combined with a global DAF.

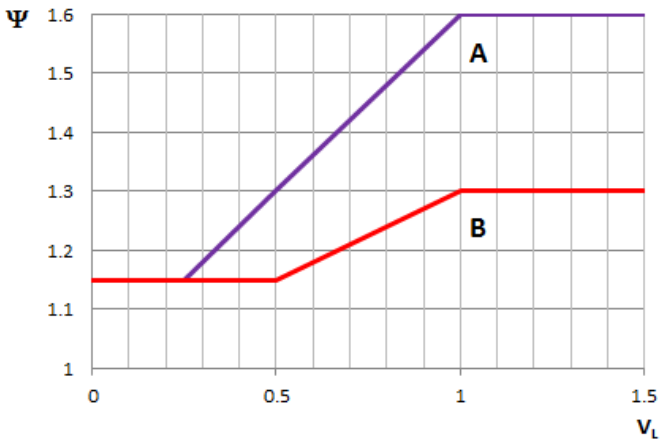

Figure 1. Dynamic amplification factor (Adapted from FEM 1.001 (1987))

This paper uses location-specific DAFs to determine the fatigue life of a 34 year-old ship unloader. As opposed to global DAF values taken from the code, location-specific DAFs are estimated from field measurements at different critical locations. For

this purpose, a low-pass filter was applied to the measured total response to obtain the maximum static response. Maximum total response was then divided by maximum static (filtered) response to obtain location-specific DAF for each measurement point. Stress ranges are evaluated using location-specific DAFs, and fatigue life was calculated based on Miner's rule and the specific dynamic behavior of each location. Results are compared to those obtained by a more conventional approach based on adopting DAF values from Figure 1.

2 DESCRIPTION OF THE SITE

2.1 *The structure*

The structure under investigation is an aged grab ship unloader, put in service in 1978 at Hunterston Terminal in Scotland. This kind of port crane is widely used to unload bulk material from different vessels.

The structural scheme of the crane and their main components is shown in Figure 2. Upper and lower substructures can be distinguished. The former is mainly composed by the ties and the boom, while the principal structural elements of the latter are the hopper and the waterside and landside portals. The part of the boom that extends beyond the waterside portal is called lifting boom while the one that extends beyond the landside portal is the rear boom. While the rear boom is fixed, the lifting boom is a retractable element, supported by the waterside ties, which are pin connected at both ends. The main grab, used to unload bulk materials, travels along a trolley installed on the boom, with a maximum outreach from the front leg of 48m and maximum back reach from the front leg of 18m. Apart from the ties, which have an I-shape section, other main structural elements have a box-type section.

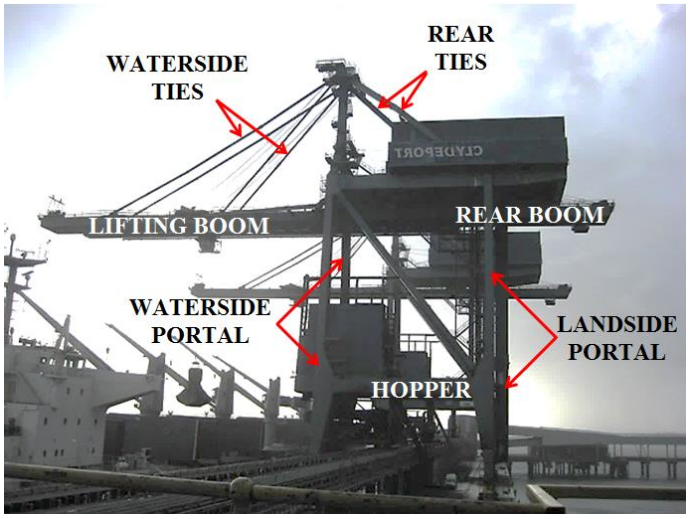

Figure 2. Main structural elements of a grab ship unloader

2.2 *The measurements*

A monitoring system was installed in 2012, to gather data while the unloader is in operation. The conceptual plan of the ship unloader in Figure 3 shows the 16 locations in which the strain gauges were installed. A total of 48 channels of strain and 4 temperature sensors were recorded. They were placed in a full bridge configuration that allowed obtaining both axial and bending stresses at each location. The data from all the channels were acquired at a scanning frequency of 125 Hz, and stored in 10-minute-binary files by a central data acquisition unit.

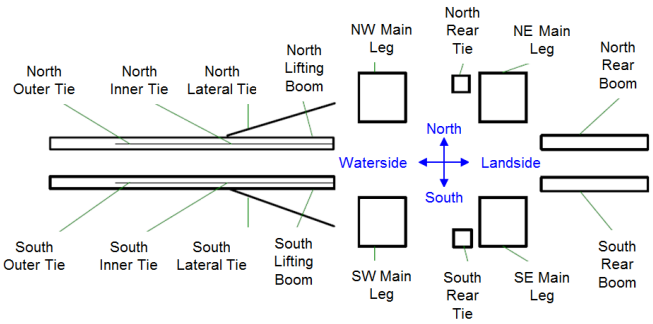

Figure 3. Location of the transducers on the ship unloader

The monitoring of the unloader took place between 10th and 26th October 2012. Over this period, five different vessels were unloaded by the crane, as shown in Table 1.

Table 1. Vessels unloaded during the monitoring period

Vessel	Date Started	Date Completed
Coronis	11/10/12 17:00	13/10/12 18:22
Pacific Breeze	13/10/12 21:50	15/10/12 18:18
Aphordite L.	16/10/12 13:00	18/10/12 14:30
Fortune Sunny	18/10/12 18:05	20/10/12 13:10
Magnolia	20/10/12 16:30	24/10/12 07:00

The vessels in Table 1 are primarily used for transporting coal and all are Panamax vessels, apart from Magnolia, which is a Capesize vessel. While the latter is a very large vessel, the former type as its name suggests, has size beam restrictions set by the dimensions of Panama Canal. In the following sections, the unloading of the Panamax vessel Coronis is analyzed.

2.3 *Dynamic properties*

Following an Operational Modal Analysis, the first two modes of vibration were found to have frequencies of 0.7845 and 0.9122 Hz. The mode shapes are represented in Figure 4. The two modes are characterized by a seaward-landward swaying of the upper substructure with relatively small lateral and twisting motion.

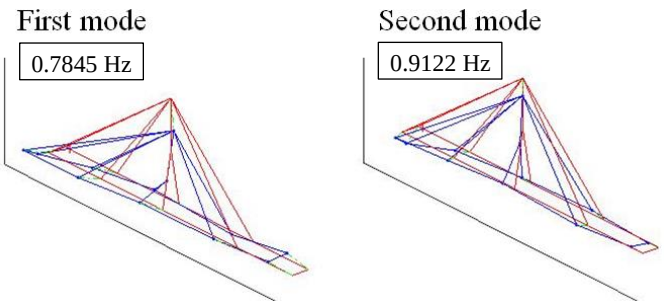

Figure 4. First two modes of vibration

3 ESTIMATION OF STATIC STRESSES

The data provided by the monitoring system was processed into strain-time histories using MATLAB®. The corresponding stresses were obtained applying a Young's module of 207 GPa. During the post processing of the data, correction factors were applied to locations in which the strain gauges were installed off center. This situation happens, for example, in the lifting boom, where strain gauges are installed above the central line of the section due to the presence of internal stiffeners.

Figure 5 shows axial stress in the inner ties between 23:26:35 and 23:28:30 on 11th October 2012, due to two cycles of the grab. The position of the grab along the boom and the hoisting speed, during this loading cycle are not known, but can be estimated from the recorded strain histories during one loading cycle. Figure 5 illustrates the approximate position of the grab along the boom for three significant instants of the cycle. It can be assumed that at approximately time=400s the empty grab starts moving from the hopper to the boom at time=425s it starts to lift the coal and then it starts to return to the hopper and drops the coal at time=455s.

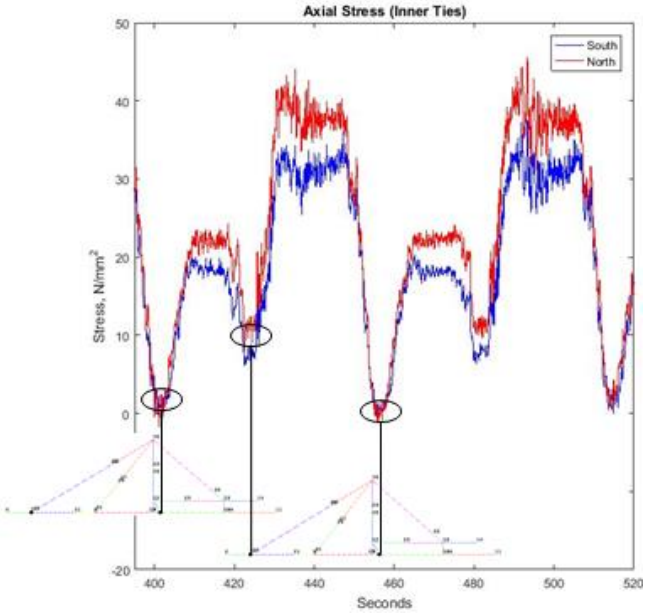

Figure 5. Measured axial stress for inner waterside ties.

An 8th order Chebyshev Type I low-pass filter was applied to the measured data in order to obtain the static response, with a cutoff frequency given by Equation 1.

$$cutoff\ frequency = 0.8 \cdot \frac{\left(f_S/_2\right)}{R} \quad (1)$$

where f_s is the sampling frequency and R is the factor used for filtering (IEEE Press, 1979).

Considering the first of the aforementioned cycles for the north inner tie, different cut-off frequencies were applied in order to identify the most suitable filter. A cut-off frequency of 0.4Hz (corresponding to R = 125) was found to efficiently remove the first mode of vibration of the ship unloader at 0.7845 Hz. A comparison between the recorded response and the static response obtained after applying the filter is shown in Figure 6.

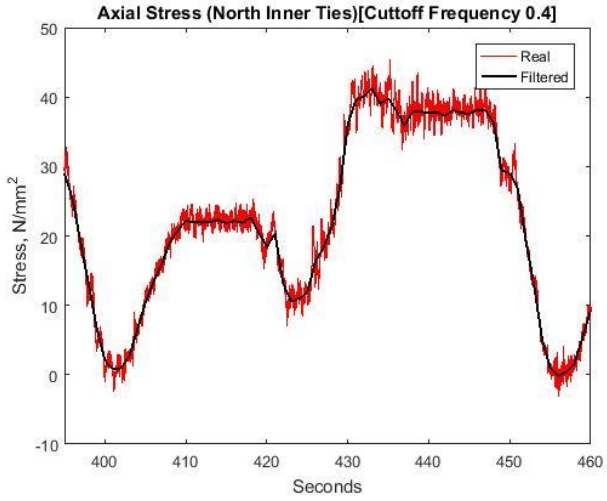

Figure 6. Comparison between measured (Real) data and estimated (Filtered) representing estimated static response.

According to Figure 1, making a conservative assumption of maximum speed above 1 m/s, the value of DAF for a grab ship unloader, was **Ψ**=1.3. In order to assess the degree of conservatism of the code, estimated static stresses were multiplied by 1.3 and are compared to the recorded stresses in Figure 7. The product of the estimated static stress by DAF is sometimes referred to as pseudo-static stress.

For some locations, such as the lateral bending stress in the waterside ties Figure 7 shows that the dynamic stress is underestimated by the pseudo-static stress.

It is worth noting that the total response was obtained by applying a cut-off frequency of 10 Hz, doing so removes the noise from the structural response.

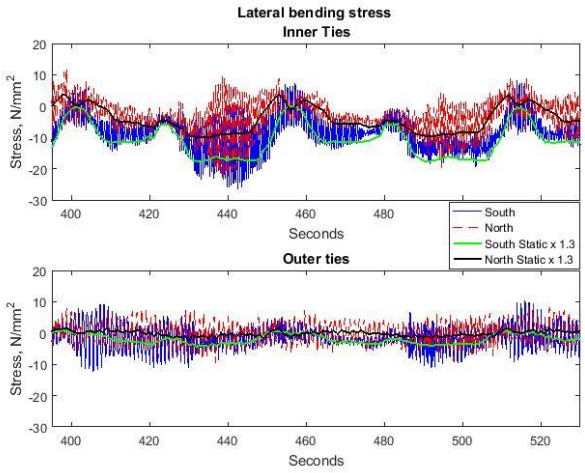

Figure 7. Comparison between measured and pseudo-static stresses for lateral bending stress in the waterside ties.

4 DESCRIPTION OF THE FE MODEL

4.1 *Geometry and loads*

A two-dimensional FE model was built using ANSYS APDL (Fig. 8). Beam elements were used to model the primary structural load bearing members. For each structural member, beam-equivalent section properties were evaluated. The secondary non-load bearing structural members, i.e. the lift and the machinery room were not modelled. The numbered nodes rounded by a circle in Figure 8 represent the locations in which the monitoring system has been installed, for which measured data is available.

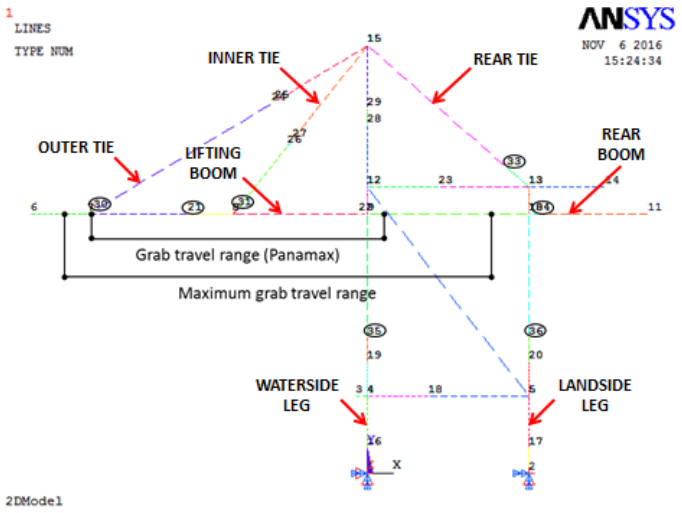

Figure 8. A 2D FE model of the ship unloader.

When unloading Panamax vessels, it has been observed that the main grab has a reduced travel range and it does not move all the way to its maximum outreach and back reach (Fig. 8). More specifically, the grab has a maximum outreach between the inner and the outer ties and a back reach of a couple of meters landside from the waterside legs. Therefore, for the vessel Coronis a travel range from the outer ties 2 meters landside to the waterside ties was considered.

Given that the Coronis is transporting coal, the total weight of the grab was calculated using the payload properties given in Table 2. Therefore the mass of the loaded grab was evaluated as 43.4 tonnes while that of the shuttle trolley as 15.37 tonnes. These values, divided by two, are applied to the FE model in Figure 8 as point loads. In fact, the entire load is carried by the north and south boom, while the FE model used here represents only one side of the structure.

Table 2. Weight of the full grab for coal payload.

Material	Density (T/m^3)	Grab capacity (m^3)	Payload (T)	Grab weight (T)	TOT weight (T)
Coal	0.899	25	22.4	21	43.4

4.2 *Static results*

The static analysis was conducted considering a number of loading cases, which refer to different positions of the main grab and the shuttle trolley along the boom. Main grab and shuttle trolley were applied to the model as point loads, and the position of the shuttle trolley was related to that of the grab through the Equation 2.

$$Y = 5.4 + \frac{(48+X)}{2} \qquad (2)$$

where X and Y represent the position of the main grab and the shuttle trolley respectively. These coordinates are expressed in meters and, as shown in Figure 9, their origin corresponds to the intersection between the boom and the waterside leg.

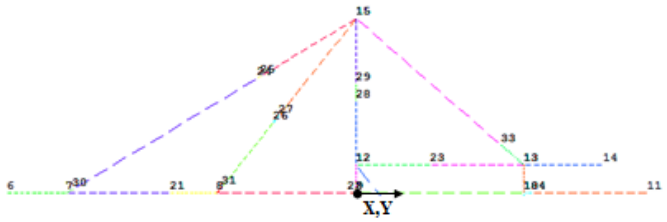

Figure 9. Reference system for the position of the grab (X) and the shuttle trolley (Y) along the boom.

Figure 10 represents the variation in stresses versus the position of the main grab along the boom for vertical bending stress in the lifting boom and axial stress in inner tie. For a better understanding of the position of the grab, a scheme of the upper substructure is shown along the x-axis.

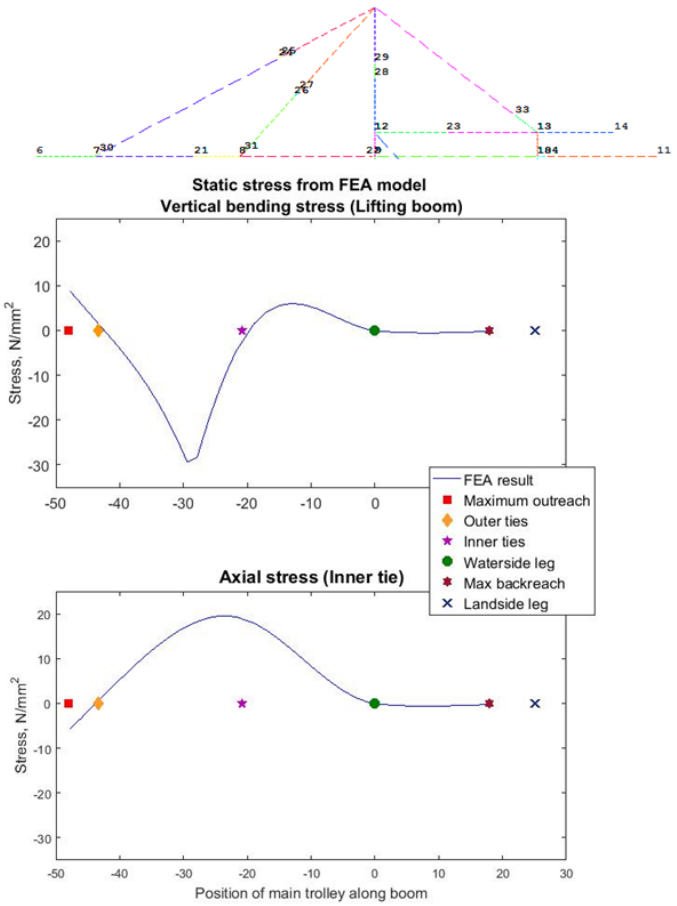

Figure 10. Static vertical bending stress from FE model

Table 3 compares the maximum measured total stress responses (after removing noise) to those obtained from pseudo-static analysis using the FE model at measured locations and global DAF values. The pseudo-static analysis has been conducted considering coal payload and a travel range corresponding to unloading Panamax vessel, and the static results have been multiplied by the DAF provided by the standard.

Table 3. Comparison between measured stresses (after removing noise), and pseudo-static stresses.

	Measured stresses (noise removed)			Pseudo-static stresses	
	Axial	Vert. Bend	Lat. Bend	Axial	Vert. Bend
Outer Ties	15.8	11.9	13.6	19.4	0.0
Inner Ties	40.0	21.6	25.9	25.4	0.0
Lateral Bracings	7.1	11.2	1.8	-	-
Lifting Boom	5.8	37.3	6.7	5.6	38.3
Rear Ties	17.6	4.0	3.4	12.7	1.0
Rear Boom	4.6	35.6	2.9	0.0	21.1
Waters. Leg	9.1	3.4	1.5	8.5	0.7
Lands. Leg	6.5	1.8	1.2	4.3	0.8

The lateral bracings lie in a plane orthogonal to the one considered and are not considered. Obviously, the 2D FE model is not able to predict the lateral bending stresses in the structural members analysed. Furthermore, the waterside ties (north and south) show unexpected bending stresses, not predicted by the FE model. As pointed out by Chang (2010) and Chang et al. (2012), this increase in stresses arises from the pin ends not free to rotate.

Figure 11 shows a comparison between the estimated static stresses (after removing noise and dynamics) and those obtained by the FE model, for axial stress in the inner ties and for vertical bending stress in the lifting boom.

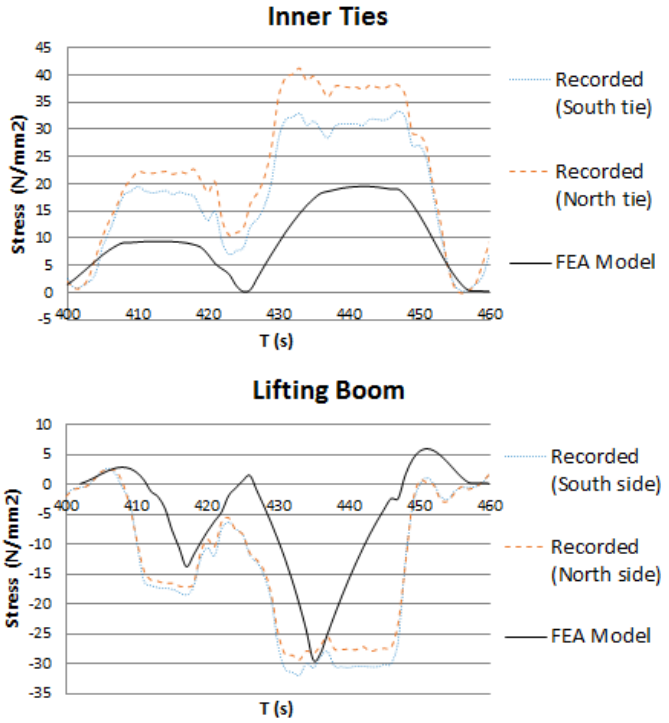

Figure 11. Comparison between the estimated static stresses and the static stresses from the FE model for axial stress in inner ties and for vertical bending stress in lifting boom.

As shown in Figure 11, the shape of the response obtained from the FE model resembles the behavior of the structure, however, a significant difference in magnitude is observed for the inner ties. While the FE model employed here cannot predict the exact behavior of all measured stresses, it is used to illustrate the process of carrying out a fatigue analysis in a real-life situation (i.e., step (1) defined in Section 1).

The purpose of the FE model is extending fatigue calculations to locations and loads other than those scenarios where and when measurements take place. The authors acknowledge that the simplified 2D FE model in this paper has limitations such as the inability to model lateral stresses or to model vertical bending in ties that are assumed to be pinned at both ends amongst others, and that in reality, a more ac-

curate 3D FE model would be needed. Therefore, the current investigation is focused only on sections that are instrumented on-site, and it does not pay attention to other potential critical locations. However, the current simplified FE model is deemed to be sufficient reproducing axial stresses to some extent at a number of measured locations, and for demonstrating the impact of using measured dynamic amplification factors on fatigue life. Again, in an ideal situation, the FE model would need to be calibrated not only statically (to reproduce all axial, vertical and lateral static stresses), but also dynamically to gather DAF and remaining number of cycles before fatigue failure, for locations with or without available measurements.

5 CALCULATION OF LOCATION-SPECIFIC DAF

Even though carrying out a transient dynamic analysis would be the best way for achieving an accurate assessment of the dynamic behavior of the structure, this requires some complex modelling that is time-consuming and calibration of model parameters that are labor-expensive and difficult to gather on site. This paper proposes to maintain the simplicity of the standard procedure based on multiplying the results of a static analysis by a DAF, but using measured DAFs at each location instead of a generalized DAF applicable to all cranes and locations. The new approach allows capturing the site-specific characteristics of each location and of the crane at hand.

In order to define DAFs as accurately as possible, several load cycles need to be considered. Among the data from the monitoring system, eleven complete cycles of grab have been identified. For each cycle, DAF at each location is calculated by selecting the maximum measured response and dividing by the maximum estimated static response (Equation 3).

$$DAF = \frac{dynamic\ recorded\ stress}{estimated\ static\ stress} \qquad (3)$$

It is worth noting that the numerator is obtained applying a cutoff frequency of 10Hz in order to remove noise from the measured signal. While, the denominator was the filtered signal using a cut-off frequency of 0.4Hz to remove dynamics. As example, Figure 12 illustrates this process for the axial stress in the inner tie. The maximum measured value was 44. 3 N/mm^2 and the maximum static value was 41. 1 N/mm^2, hence, the resulting DAF is equal to 44.3/41.1 = 1.08.

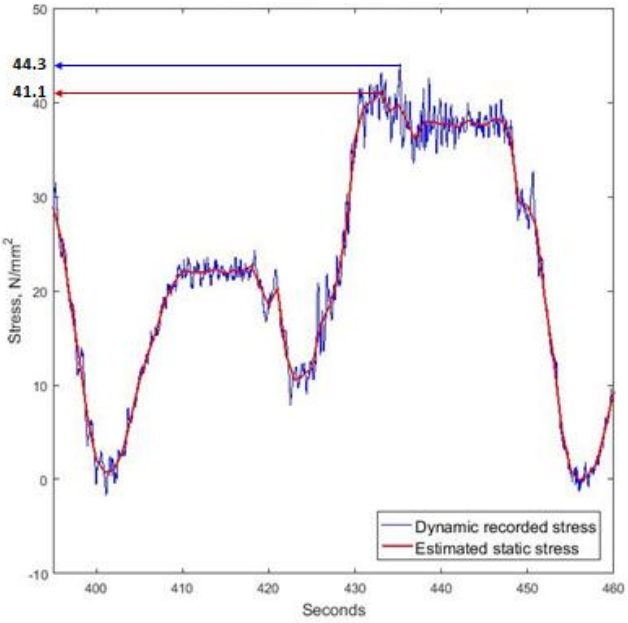

Figure 12. Process to define location-based DAF for axial stress in inner ties.

The process illustrated above, was repeated for each location and stress considered. Figures 13-15 show the values of these DAFs for axial stress, vertical bending stress and lateral bending stress respectively. Each DAF value corresponds to one of the 11 load cycles plotted on the x-axis. For reference purposes, the horizontal line in each graph represents the DAF provided by the standard. As can be seen from Figure 13, referring to axial stress, the lifting boom appears to have the biggest dispersion. In fact, it has a wide range of values between 1.3 and 3.2. For the majority of the other locations, the trend could be approximated by a straight line.

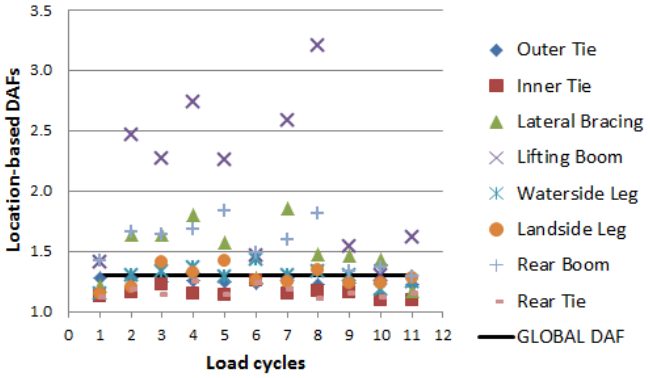

Figure 13. Location-based DAFs for axial stress.

Figure 14 shows the values of DAF of vertical bending stress; in this case the waterside and landside legs experience the biggest fluctuations.

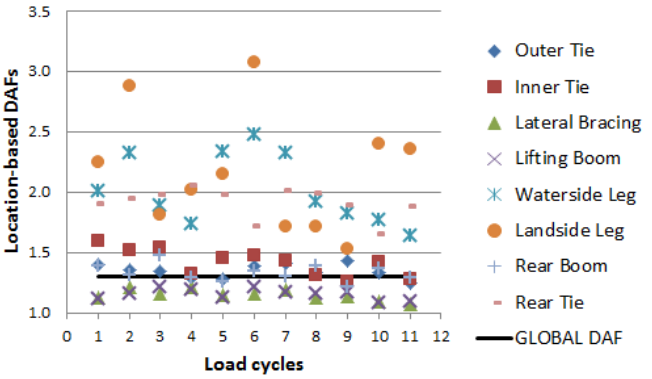

Figure 14. Location-based DAFs for vertical bending stress.

The last graph in Figure 15 plots the value of the location-based DAFs for the lateral bending stresses. Here, the outer tie, inner tie and lateral bracings presented the most significant scattering. As already shown in Figure 7, the waterside ties showed unexpected lateral bending stresses and a highly dynamic behavior. That could arise from the damage to the pins (connecting them to the lifting boom) that are not free to rotate, inducing additional stresses in the ties.

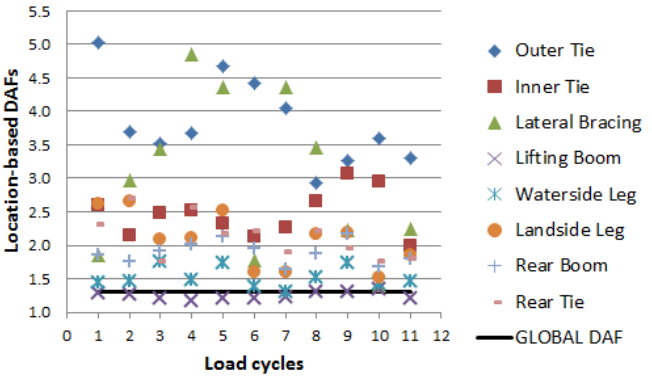

Figure 15. DAFs for lateral bending stress.

For the scenario under investigation, DAF provided by the standard was not considered representative of the real behaviour for the majority of the structural elements considered, when referring to the different component of the stress. It has been observed that some locations are more prone to dynamic amplification than others. For example, the lifting boom, the waterside ties and the legs. Therefore, this aspect of location dependency in DAF is introduced in the next section to assess the impact on the calculation of the remaining fatigue life.

6 CALCULATION OF FATIGUE LIFE USING LOCATION-SPECIFIC DAF

The stress ranges for all locations were evaluated to carry out a fatigue life assessment. Initially, the axial and bending stresses were combined to evaluate the stresses at each corner of the structural members. After that, the maximum amplitude was evaluated to establish the stress range. Then, location-based DAFs were applied to each component of stress. This procedure was repeated for each location and load cycle, leading to the values plotted in Figure 16.

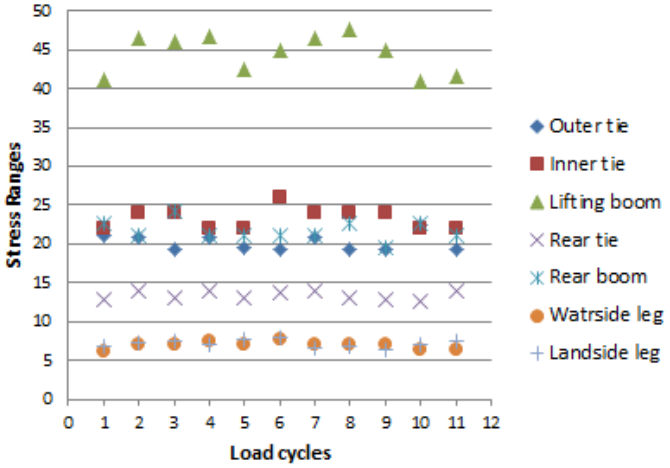

Figure 16. Stress ranges for each location and load cycle considered.

Figure 17 compares the stress ranges obtained applying the location-based DAFs to that obtained applying the global DAF by the standard for two representative locations.

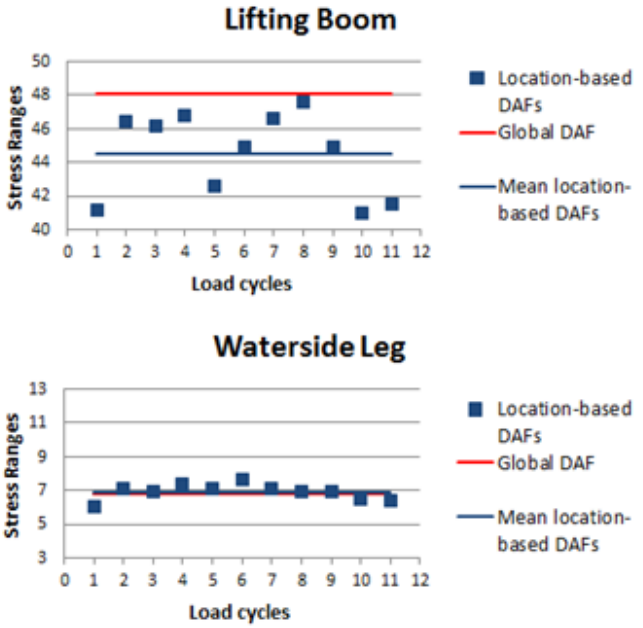

Figure 17. Stress ranges for two significant locations

The values using location-based DAFs can be more or less scatter and more or less conservative than the ones applying global DAF depending on the location under investigation. For a better understanding of the introduction of these factors in fatigue life assessment, an example evaluation of the remaining

load cycles was conducted. For each location, the mean value of the stress ranges was evaluated and Miner's rule applied to evaluate the cumulate damage corresponding to a single cycle at that stress range. Consequently, the remaining life for each location was evaluated identifying all locations as class F2, and using the corresponding fatigue strength curves provided by the British Standard 7608 (BS7608:1993). Figure 18 is the result of evaluating the number of remaining cycles for each location.

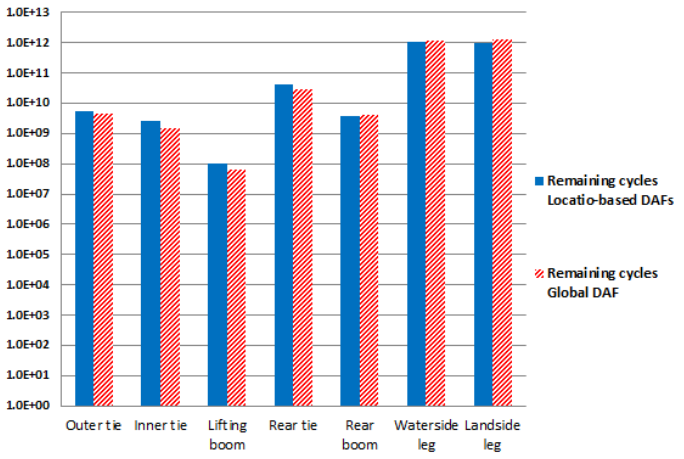

Figure 18. Remaining cycles considering a single cycle.

The histogram in Figure 18 shows that, for the lifting boom, the waterside and rear ties, the number of cycles estimated adopting location-based DAFs is higher than that obtained applying a global DAF. In the latter, the DAF provided by the standard were conservative, but adopting location-based DAFs was possible to achieve a more accurate assessment of the structure, that would ensure a safe operational condition and an extension of its life. Conversely, for the rear boom and the legs, the global DAF by the standard were not conservative according to the measurements.

7 CONCLUSIONS

The investigation carried out in this paper intends to be a starting point for more accurate future fatigue life assessments allowing for changes in dynamic amplification factor within different structural sections of a ship unloader. Even though this paper has several limitations due to the accuracy of the FE model, the measurement errors, the size of the sample and the estimation of remaining cycles, it has served the purpose of demonstrating how the remaining number of cycles can be extended or decreased with respect to the standard by considering the unique dynamic features of each section.

8 ACKNOWLEDGMENTS

This project has received funding from the European Union's Horizon 2020 research and innovation programme under the Marie Skłodowska-Curie grant agreement No. 642453 (http://trussitn.eu).

9 REFERENCES

ANSYS® Mechanical APDL, Release 14.0.

British Standards Document 7608: 1993. Code of practice for fatigue design and assessment of steel structures.

Chang, Y.F. 2010. Fatigue life evaluation of a grab ship unloader. China Steel Technical Report 23:36-41.

Chang, Y.F. & Wang, T.Y. 2012. The evaluation of fatigue crack propagation on a grab unloader. Australasian Structural Engineering Conference (ASEC 2012). Perth, Western Australia 11-13 July 2012.

Digital Signal Processing Committee of the IEEE Acoustics, Speech, and Signal Processing Society (eds.) 1979. *Programs for Digital Signal Processing* Chap. 8. New York: IEEE Press.

Federation Europeenne de la Manutention (FEM). Revised 1987.1.001. Rules for the Design of Hoisting Appliances. 3rd Edition.

MATLAB Release 2016a, The MathWorks, Inc., Natick, Massachusetts, United States.

Milana, G. Banisoleiman, K. Gonzalez, A. 2016a. Fatigue life assessment methods: the case of ship unloaders. 1st International conference on natural hazards & infrastructure (ICONHIC2016). 28th -30th June 2016. Chania: Greece.

Milana, G. Banisoleiman, K. Gonzalez, A 2016b. Sources of structural failure in ship unloaders. ESREL2016. 25th -29th September 2016. Glasgow: UK.